Machine Learning Ensemble Reveals Distinct Molecular Pathways of Retinal Damage in Spaceflown Mice

James A. Casaletto[1][*], Ryan T. Scott[2], Aahan Rathod[3], Aarav Jain[4], Aarthi Chandar[5], Aditi Adapala[6], Aditya Prajapati[7], Agastya Nautiyal[5], Anagha Jayaraman[8], Ananya Boddu[5], Anish Kelam[9], Anishka Jain[10], Bella Pham[11], Dhruv Shastry[12], Diya Narayanan[5], Eashan Kosaraju[13], Elior Paley[14], Fabian P. Uribe[15], Ibrahim Shahid[16], Isabel Ye[5], Jessica Wu[17], Joshua Lin[18], Krithikha Srinivas[19], MarcAnthony Paolieri Della Monica[20], Margaret Hitt[14], Matthew Lin[6], Maxwell Volkan[21], Misha Kharya[22], Mrinalini Kaul[23], Muhammad A. Jaffer[24], Mushtaq Ali[25], Naomi Z. Chang[26], Nishant Ashri[27], Noélie Boquet Couderc[28], Phani Paladugu[1], Ronak Hiremath[29], Rudransh Pathak[30], Saanvi Dogra[31], Samarth Srinivas[32], Shawnak Samaddar[33], Shrikar Gopinath[34], Shriya Sawant[33], Sophie Cai[35], Vania Pala[36], Vinitha Nair[5], Zhihan Shi[37], Sunny Narayanan[38], Daniya Mundackal Thomas[39], Anna Lewkowicz[40], Ethan Waisberg[41], Joshua Ong[42], Samrawit Gebre[43], Jonathan M. Galazka[43], Parag A. Vaishampayan[43], Lauren M. Sanders[1], Xiao Wen Mao[44]

Affiliations

[1] Blue Marble Space Institute of Science, Space Biosciences Division, NASA Ames Research Center, Moffett Field, CA 94035, USA.
[2] Amentum, Space Biosciences Division, NASA Ames Research Center, Moffett Field, CA 94035, USA.
[3] Mountain House High School, Mountain House, CA 95391, USA.
[4] Evergreen Valley High School, San Jose, CA 95148, USA.
[5] Lynbrook High School, San Jose, CA 95129, USA.
[6] University of California, Berkeley, Berkeley, CA 94720, USA.
[7] Thomas S. Wootton High School, Rockville, MD 20850, USA.
[8] Dunlap High School, Dunlap, IL 61525, USA.
[9] Innovation Academy, Alpharetta, GA 30009, USA.
[10] Purdue University, West Lafayette, IN 47907, USA.
[11] Cypress Ranch High School, Cypress, TX 77433, USA.
[12] Columbus High School, Columbus, GA 31904, USA.
[13] Solon High School, Solon, OH 44139, USA.
[14] Columbia University, New York, NY 10027, USA.
[15] University of Illinois Urbana-Champaign, Champaign, IL 61820, USA.
[16] The Early/Middle College at the University of North Carolina, Greensboro, NC 27410, USA.
[17] University of Rochester, Rochester, NY 14627, USA.
[18] San Marino High School, San Marino, CA 91108, USA.
[19] Tomball Memorial High School, Tomball, TX 77377, USA.
[20] University of California, Irvine, Irvine, CA 92612, USA.
[21] University of Tokyo, Kashiwa City, Chiba 277-0827, Japan.
[22] Valley Christian High School, San Jose, CA 95111, USA.
[23] Mount Olive High School, Flanders, NJ 07836, USA.
[24] George Ranch High School, Richmond, TX 77469, USA.
[25] University of Wisconsin Madison, Madison, WI 53706, USA.

26 Stony Brook University, Stony Brook, NY 11790, USA.
27 Charlotte Latin School, Charlotte, NC 28277, USA.
28 Harrison High School, Harrison, NY 10528, USA.
29 Dublin High School, Dublin, CA 94568, USA.
30 Stanford University, Stanford, CA 94305, USA.
31 Del Norte High School, San Diego, CA 92127, USA.
32 New Tech High at Coppell, Irving, TX 75063, USA.
33 Georgia Institute of Technology, Atlanta, GA 30332, USA.
34 The Lawrenceville School, Lawrenceville, NJ 08648, USA.
35 University of Michigan, Ann Arbor, MI 48109, USA.
36 Carlmont High School, Belmont, CA 94002, USA.
37 Johns Hopkins University, Baltimore, MD 21218, USA.
38 Florida State University, Tallahassee, FL 32304, USA.
39 Austin Community College, Austin, TX 78752, USA.
40 ETH Zurich, Zürich, 8092, Switzerland.
41 University of Cambridge, Cambridge, CB2 1TN, United Kingdom.
42 University of Michigan, Kellogg Eye Center, Ann Arbor, MI 48105, USA.
43 Space Biosciences Division, NASA Ames Research Center, Moffett Field, CA 94035, USA.
44 Loma Linda University Health, Loma Linda, CA 92354, USA.

Corresponding author: James A. Casaletto

Abstract

Spaceflight-associated neuro-ocular syndrome (SANS) threatens astronaut health during long-duration missions, yet its molecular pathology remains unclear. Two physiological pathways exist: one attributes SANS to microgravity-induced cephalic fluid shift causing increased intracranial pressure, altered CSF flow, blood-brain barrier disruption, and optic disc edema; the other emphasizes radiation-induced oxidative stress affecting electrolyte channels. However, the exact mechanisms are not completely understood in this unique pathophysiologic barrier to human spaceflight. We investigated two cellular stress markers in the retinal tissues of mice (n=16) flown on the International Space Station (ISS): 4-hydroxynonenal (4-HNE), indicating oxidative stress and lipid peroxidation, and DNA fragmentation detected via TUNEL assay, indicating apoptosis. Using an ensemble of five machine learning algorithms to analyze gene expression profiles, we identified genes that are most predictive of 4-HNE and TUNEL phenotype values. By identifying the most predictive protein-coding genes, we identified associated molecular pathways whose dysregulation may mechanistically link spaceflight conditions to SANS-related retinal damage. Our findings support oxidative stress and DNA damage as primary drivers in SANS pathology. This computational approach uses robust correlation to reveal pathway associations that may inform future therapeutic investigations, advancing our understanding of SANS molecular mechanisms, and offering potential intervention strategies for protecting astronaut vision during future deep-space missions.

Introduction

Prolonged microgravity exposure produces multiple physiological and pathological changes within astronauts [1], many constituting SANS. This syndrome encompasses changes in

ophthalmologic tissues during long-duration spaceflight, including optic disc edema, posterior globe flattening, choroidal thickness changes, retinal folds, and oxidative damage within the blood-brain barrier [2-4]. These manifestations pose serious risks during long-term missions and represent obstacles to future deep space exploration. SANS prevalence among astronauts is high. Approximately 70 percent of ISS astronauts reported posterior eye swelling, with over 45 percent reporting near distance visual acuity changes during missions exceeding 30 days, compared to 23 percent experiencing symptoms during shorter exposures [3,4]. Structural changes, visual acuity discrepancies, and magnetic resonance imaging findings consistently demonstrate SANS pathology [2,4,5]. There are predominantly 2 pathways which are hypothesized to drive SANS pathologies: cephalad fluid shifts due to microgravity; and oxidative stress due to radiation exposure.

Microgravity-induced cephalad fluid shifts represent a key mechanism underlying SANS pathophysiology [4,5]. During ascent, cephalic, cervical, and pectoral tissues swell while femoral and abdominal regions slim. Upon reaching orbit, fluids achieve homeostatic distribution maintained throughout missions [5]. This redistribution triggers pathological cascades. Venous congestion increases ocular venous pressure, contributing to choroidal expansion through vortex vein drainage lacking autoregulatory control [5,6]. Choroidal expansion also occurs during head-down tilt parabolic flights [4,5]. Cephalad fluid shift causes optic disc edema and contributes to optic disc protrusion and osteoma-like formations [2,4].

Beyond hemodynamics, microgravity and space radiation elicit retinal oxidative stress and apoptosis underlying SANS alterations. Murine studies demonstrate elevated 4-HNE and increased TUNEL-positive nuclei in the inner nuclear layer (INL) and ganglion cell layer (GCL) following ISS exposure and simulated radiation [3], with additional evidence of adverse photoreceptor and retinal functional changes [7]. Reactive oxygen species (ROS) trigger lipid peroxidation producing electrophilic aldehydes like 4-HNE. Caspase activation drives DNA fragmentation detectable through the TUNEL assay [8].

A 35-day ISS mission with C57BL/6 mice revealed over 600 differentially expressed retinal genes enriched for visual perception, phototransduction, and photoreceptor phenotypes, with 286 upregulated and 314 downregulated genes correlating with retinitis pigmentosa, diabetic retinopathy, macular degeneration, and retinal detachment [9]. 4-HNE staining increased in cone photoreceptors, INL, and GCL post-spaceflight [10]. TUNEL assays provided first evidence of space-induced oxidative damage from mitochondrial apoptosis [3]. Despite these observations, molecular circuitry linking transcriptomic remodeling to oxidative injury and apoptosis within SANS remains undefined. Previous studies treated RNA sequencing, histology, and imaging as parallel endpoints without identifying quantitative linkage between gene expression patterns and oxidative stress assays [3]. To address this gap, we applied a multi-modal machine learning ensemble that integrates retinal transcriptomic profiles with quantitative bioimaging phenotypes (4-HNE immunoreactivity and TUNEL labeling) from spaceflight-exposed and ground control samples to identify consensus gene signatures predictive of tissue-level oxidative injury and apoptosis.

Methods

We developed a multi-modal machine learning pipeline to identify genes whose expression profiles predict quantitative bioimaging phenotypes of retinal oxidative stress and apoptosis. Figure 1 summarizes the complete workflow; the following subsections detail each stage.
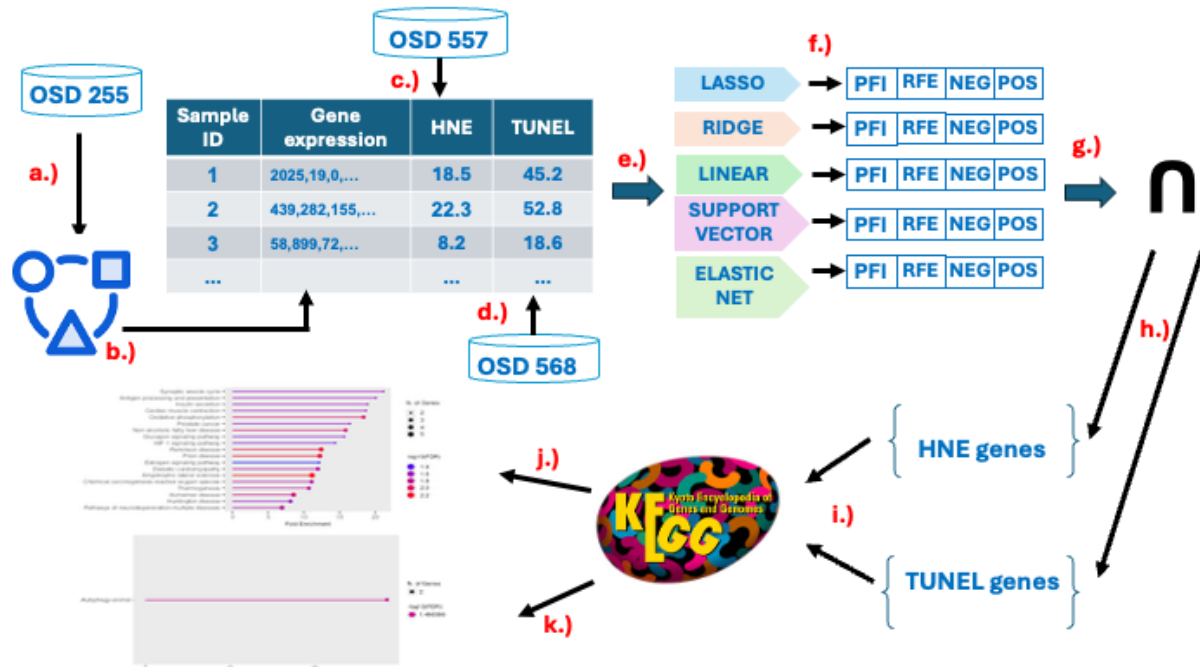

Figure 1 Machine learning pipeline. a.) Combined RSEM and STAR abundance data from OSD-255. b.) Applied filters and data transformations to prepare for training models. c.) Assigned HNE phenotype values and gene expression data for each sample. d.) Assigned TUNEL phenotype values and gene expression data for each sample. e.) Trained ensemble of linear regression models to predict phenotype values. f.) Identified genes most predictive of phenotype values for each model using permutation feature importance (PFI), recursive feature elimination (RFE), largest positive coefficients, and largest negative coefficients. g.) Found the intersecting majority consensus of most predictive genes across all models in ensemble. h.) Identified genes uniquely predictive of TUNEL and HNE phenotypes and sent them to the KEGG database to obtain enriched gene sets for i.) HNE and j.) TUNEL.

Data

The Rodent Research 9 (RR-9) mission, conducted by NASA in August 2017, investigated these effects using murine model organisms, with initial characterization demonstrating blood-retinal barrier disruption and ocular adaptations [11]. Two datasets from this mission were collected and curated by the NASA Ames Life Sciences Data Archive [12], and one dataset was curated by NASA GeneLab, all three now accessible through NASA's Open Science Data Repository [13]. OSD-557 and OSD-568 contain bioimaging data which explore the retinal consequences of spaceflight using 4-HNE immunofluorescence to assess oxidative stress and TUNEL bioimage staining to detect apoptosis, respectively [14,15]. These studies aimed to elucidate molecular and cellular mechanisms underlying SANS to inform potential therapeutic strategies. Complementing the imaging data, OSD-255 provides bulk RNA sequencing-derived gene expression profiles

from retinal tissue [16]. There were 16 male C57BL/6J 10 week-old mice in this experiment. Eight of the mice were flown in space for 35 days with a 12-hour light/dark cycle. They were fed nutrient-upgraded rodent food bars *ad libitum*, sacrificed in flight, and frozen using liquid nitrogen. The eight ground control mice were otherwise exposed to identical conditions.

In OSD-255, RNA-seq was performed using single-stranded, ribo-depleted sequencing with an External RNA Controls Consortium (ERCC) spike-in mix on an Illumina HiSeq 4000. The sequencing data were trimmed using TrimGalore and aligned using both RNA-seq by Expectation-Maximization (RSEM) and Splice Transcripts Alignment to a Reference (STAR) software [17, 18]. We merged both gene expression data files (unnormalized STAR counts and unnormalized RSEM counts) as predictors in our model. In OSD-557, oxidative stress was evaluated using 4-HNE immunostaining, a marker of lipid peroxidation. ImageJ analysis quantified HNE-positive cells and immunofluorescence intensity in the cone photoreceptors, INL, and GCL. Key metrics assessed included total HNE-positive cells (`sumcount`), HNE-positive endothelial cells (`sumEC`), and endothelial cell density (`denEC`). For OSD-568, TUNEL assays were used to label DNA fragmentation, a hallmark of apoptosis, in stained retinal sections from spaceflight and ground control mice. The CellProfiler software package quantified TUNEL-positive nuclei, focusing on the GCL, INL, and outer nuclear layer (ONL), to provide insight into regional apoptotic activity. For our machine learning models, we isolated the endothelial cell-specific phenotype variables (total EC is `sumEC` and EC density is `Density_EC`) since they directly align with the study's focus on how stress on retinal capillaries can compromise the blood-retinal barrier (BRB) and lead to retinal degeneration.

Figure 2 shows the box-and-whisker plots of the distributions of HNE `sumEC` and TUNEL `Density_EC` phenotype measurements in the ground control and spaceflight groups. Using the Students t-test, we found that the difference between the means of the ground control and spaceflight distributions for both phenotypes is statistically significant (p<0.05).
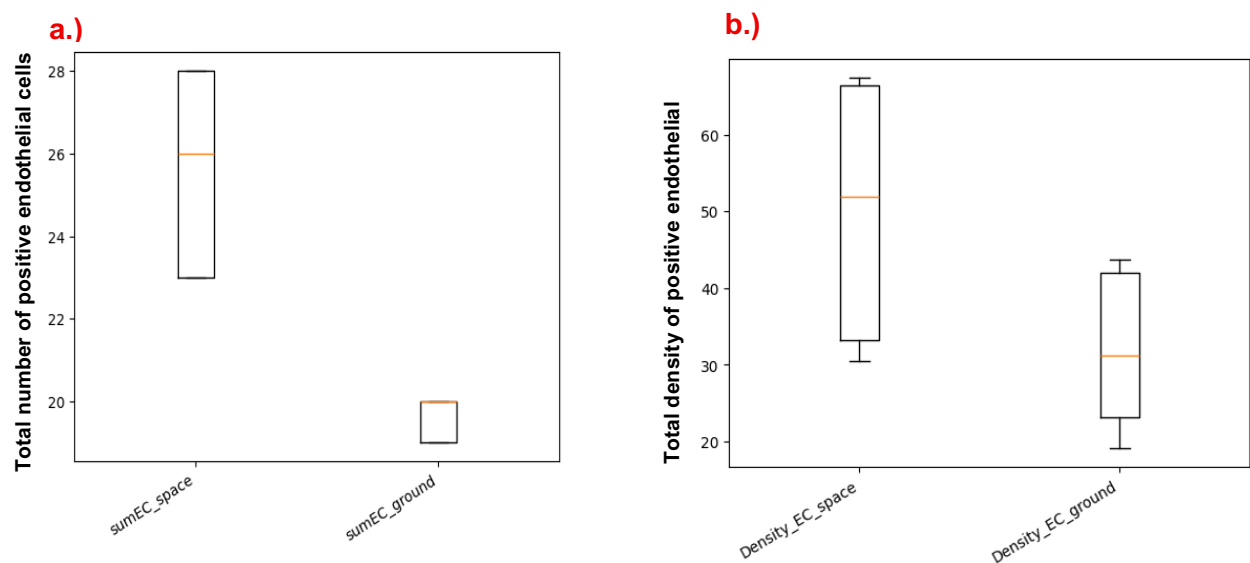
Figure 2. a.) Distributions of HNE phenotype measurements (`sumEC`) on a scale from 0 to 30 for spaceflown mice and ground control mice. b.) Distributions of TUNEL phenotype measurements (`Density_EC`) on a scale from 0 to 70 for spaceflown and ground control mice.

Data Preparation

RSEM and STAR are included in the GeneLab transcriptomic processing pipeline [19,20]. We merged both files as a form of data augmentation to help offset the high dimensionality of our gene expression data. First we removed genes that did not have counts for all samples. Next, we removed low-abundance genes from the data with a threshold of 50 or fewer transcripts in 80% or more of the samples. We considered only protein-coding genes for two reasons: first, we wanted to use downstream bioinformatic tools to analyze the resulting gene sets, and those tools are mostly annotated for protein-coding genes; and second, we wanted to identify genes with potentially therapeutic targets. Finally, we kept the 1,000 genes most highly correlated to the phenotypic target. Table 1 depicts the number of genes removed by each filter.

Filter name	Number of genes before applying filter	Number of genes removed by filter	Number of genes remaining after filter
Filter NaNs	56,840	33,421	23,419
Filter lowcount	23,419	12,477	10,942
Filter non-coding	10,942	553	10,389
Filter non-correlated	10,389	9,389	1,000

Table 1. Filters applied to the data to reduce dimensionality, beginning with 56,840 genes and ending with 1,000 genes for all the experiments.

In addition to filtering the data, we performed the following transformations before training the model. First, we normalized the data using transcripts per million (TPM) to account for sequencing depth and gene lengths. Second, we scaled the data to z-scores so that we can use coefficient-based feature importance methods.

The PCA plots of Figure 3 show clearly separated sample gene expression clusters for high and low values of the HNE and TUNEL phenotypes. This suggests that gene expression may be used to predict the phenotype values for each assay.
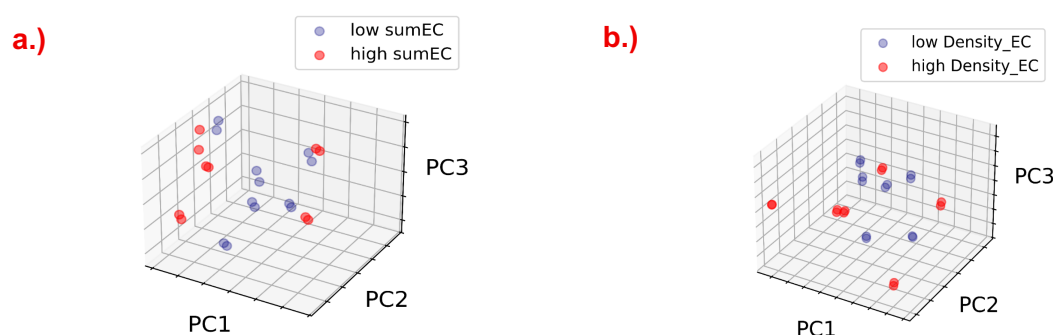
Figure 3. PCA plots of gene expression data colorized by low and high phenotype values for a.) HNE `sumEC` and b.) TUNEL `Density_EC`. Each sample has 2 closely paired gene expression values (one from STAR protocol and one from the RSEM protocol).

Machine Learning Ensemble

To investigate whether spaceflight-induced retinal stress can be detected directly from transcriptomic signatures, we built a multi-modal machine-learning ensemble to predict 4-HNE and TUNEL phenotypes from gene expression profiles. The goal of this research is to determine whether transcriptomic patterns could reliably predict oxidative damage (4-HNE) and apoptotic activity (TUNEL). The use of multiple linear regression models captures linear signatures of retinal injury induced by spaceflight. By combining models that each learn biological signals in different ways, the ensemble provides a more comprehensive and robust estimate of gene-phenotype relationships than any single method alone. We adapted the ensemble machine learning methodology of Casaletto et al. [21], which employed multiple linear classifiers and majority voting to identify consensus gene sets predictive of spaceflight-induced phenotypic changes.

We chose 5 different machine learning models to form our ensemble: linear regression, elastic net, support vector regression, ridge regression, and lasso regression. The basic form of linear regression estimates a continuous response from a linear combination of predictor variables, through estimating coefficients by minimizing the sum of squared residuals between observed and predicted values [22]. Support vector regression uses a kernel-based approach that fits a function within a margin of error and maximizes the margin around it to show linearly or non-linearly separable relationships between the inputs and the target, depending on the choice of kernel [23]. Ridge regression adds an L2 penalty (proportional to the squared magnitude of the coefficients) to the least squares loss, which shrinks coefficient magnitudes towards zero. This reduces multicollinearity and overfitting in high-dimensional settings [24]. Lasso regression adds an L1 penalty on coefficient magnitudes, driving many coefficients to exactly zero, which effectively performs feature selection and identifies the most predictive variables in the dataset [25]. Elastic net regression combines the penalties of both L1 (lasso) and L2 (ridge) regularization so that it shrinks coefficients and performs variable selection. This is especially useful when predictors are highly correlated [26].

Using an ensemble of regression models instead of relying on a single model provides the benefit of being able to leverage the various unique strengths of each algorithm and reduce model-specific bias or variance, particularly with a high-dimensional feature space such as gene expression data [21]. Each regression method learns patterns in its own way. For example, regularized models like ridge, lasso, and elastic net limit the influence of weak or noisy genes, whereas support vector regression uses kernel functions to define boundary relationships. Together, the ensemble can model both simple and complex gene-phenotype patterns. Ensemble learning often improves reliability in small, high-dimensional biological datasets where no single model performs best across all conditions. All five models were built using `scikit-learn` version 1.7.2.

Model Selection

We used a train/test split of 70/30 and validated using k-fold cross validation across the training data. This ensures that each sample is used for both training and validating and reduces overfitting. It also has the effect of giving a more stable estimate of performance [27]. Because our dataset is so small, we used the leave-p-out (p=2) method of cross-validation for model selection. This method is ideal for small datasets because it makes efficient use of limited samples and provides a more stable estimate of model performance. To assess the quality and generalisation capacity of the regression models, we calculated the R^2 (coefficient of determination). This metric, calculated with the `scikit-learn` library, provides an evaluation of the models' explanatory power and absolute magnitude of prediction error. The R^2 score is a measurement that quantifies the proportion of the variance in the dependent variable (the phenotype values) that the model predicts given the independent variables (the gene expression profiles). The R^2 score serves as a relative measure of model fit, comparing the model's performance to a baseline prediction of the mean of the observed data. A score of 1.0 indicates a perfect prediction, with the model explaining 100% of the variability in the target data. A score of 0.0 indicates the model performs no better than the baseline, and a negative score indicates the model performs worse than simply predicting the mean of the target values. We selected the models with an R^2 score of 0.9 or higher as a conservative threshold based on an informal assessment of R^2 score thresholds defined in the scientific literature. After training each model, we identified the features most predictive of the phenotype values on the held-out test data using the feature-selection methods described below.

Feature Selection

We used two approaches from the `scikit-learn` package for feature selection using the test data set: PFI and RFE. The PFI approach randomly permutes the values of each feature across the test samples one by one and calculates the model performance before and after having done so, which measures how much each feature affects model performance [28]. The degree to which the model performance changes is assigned to each feature as its importance metric, with larger degradations indicating greater importance. RFE, by contrast, repeatedly removes the least predictive features from the model through an iterative retraining process, revealing which features are most important to the model's internal predictive structure. The algorithm continues rebuilding models and removing features until the desired number of features remain [29]. Using both PFI and RFE allows us to capture complementary information: PFI reflects a feature's external impact on model performance; and RFE identifies features that the model internally depends on most. For both feature selection techniques, we used the coefficient of determination

scoring metric R^2. We also used coefficient magnitude to identify the features with the largest coefficients as a proxy for feature importance. We selected the 40 largest magnitude positive coefficients and the 40 largest magnitude negative coefficients. In summary, each ML algorithm generates 4 lists of 40 genes: genes ranked by PFI; genes ranked by RFE; genes associated with the 40 largest positive coefficients; and the genes associated with the 40 largest negative coefficients.

We intersect the PFI and RFE gene sets, then intersect that result with the union of the positive and negative coefficient sets. Positive coefficients were interpreted as features whose higher values are associated with an increase in the predicted outcome (assumed to be "up-influencing" the response), while negative coefficients indicate features whose higher values are associated with a decrease in the response (assumed to be "down-influencing" the response). Intersecting these lists increases stability and reproducibility by ensuring a gene must be consistently important across multiple, independent criteria rather than appearing due to noise in any single method. We keep the genes that appear in the list of the simple majority of the models whose R^2 performance is higher than 0.9 to define the final list of genes for the ensemble, only keeping genes that are repeatedly selected by high-performing models in the final ensemble list. This cross model comparison reduces model-specific bias or noise and emphasizes features that are stable and robustly predictive across methods.

Gene Set Enrichment Analysis

Our bioinformatic pipeline concludes with gene set over-representation, enrichment, and pathway analysis. Predictive genes from machine learning models underwent gene set enrichment analysis using the online Web portal for the Molecular Signatures Database (MSigDB) against Gene Ontology collections (biological process, molecular function, cellular component) and Human Phenotype Ontology sets. MSigDB enrichment tests whether predictive genes cluster significantly within curated gene sets representing pathways, functions, processes, and phenotypes [30]. This overrepresentation test counts overlap between our lists and curated sets, computes p-values, and applies multiple testing corrections (FDR < 0.05). No enrichment score thresholds were applied. We leveraged MSigDB to link gene lists to known biological contexts: 4-HNE-only genes (oxidative stress and vascular pathways); TUNEL-only genes (apoptosis and retinal degeneration pathways); and genes overlapping in both (neurovascular dysfunction).

Comparison to causal inference ensemble

We compare the results of our machine learning ensemble to the results from a known causal inference platform called the Causal Research and Inference Search Platform (CRISP). CRISP itself is an ensemble of 4 machine learning algorithms which leverages the concept of invariance as an *in silico* proxy for causality. Casaletto et al used the CRISP platform to identify genes putatively causal of non-alcoholic fatty liver disease in spaceflown murine liver tissue [31].

Results

In this section, we discuss the training, testing, and validation performance of each of the models in the ensemble. We then describe the genes that our ensemble identified as most predictive of

the HNE and TUNEL phenotypes. Finally, we discuss the gene sets that are most enriched by the most predictive genes for the HNE phenotype, TUNEL phenotype, and for both phenotypes.

4-HNE model performance

Figure 4 shows the distributions of cross-validation and held-out test R^2 scores for the HNE phenotype. We include the most predictive genes only from those models whose held-out test R^2 scores are 0.9 or higher and then take the genes that appear in a simple majority of those high-performing models as our final gene sets.

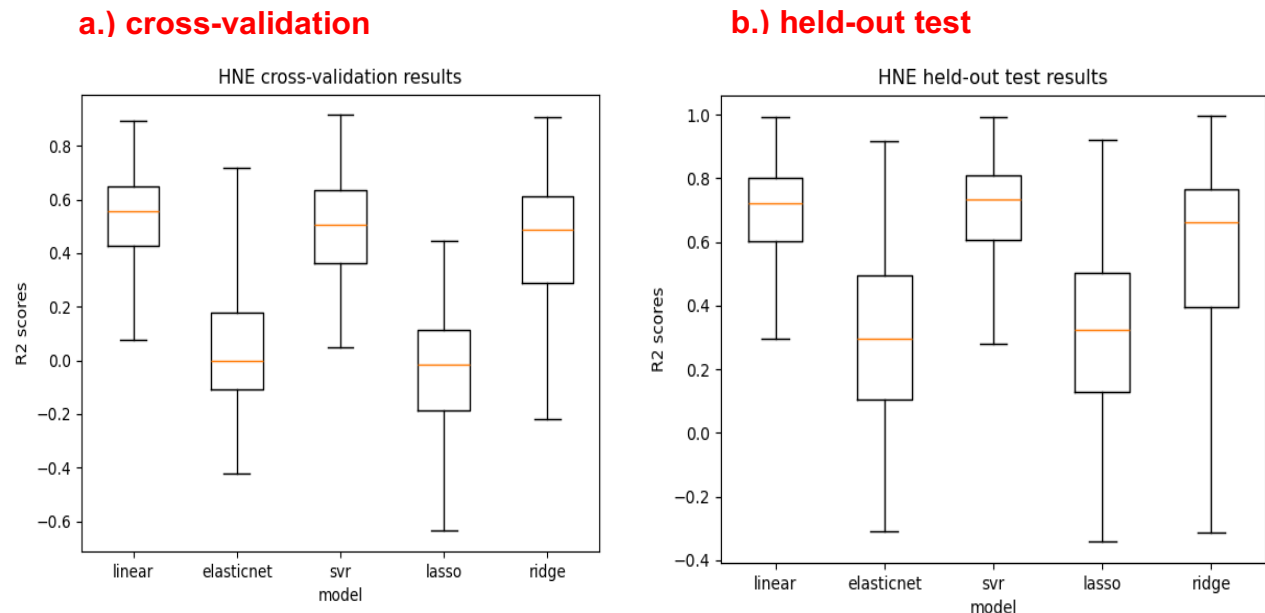**a.) cross-validation**   **b.) held-out test**

Figure 4. Performance results from the a.) cross-validation set and b.) held-out test set for each regression model predicting the 4-HNE phenotype value.

In the case of 4-HNE, three of the five models achieved R^2 scores higher than 0.9 (linear regression, lasso regression, and ridge regression). In the construction of the final gene set for 4-HNE, we select those genes which appear in the majority (2 or 3) of feature importance lists of these 3 algorithms. As shown in Figure A1 of the Appendix, the genes most predictive of the 4-HNE phenotype values are approximately uniformly distributed across the background of all genes, demonstrating that the results are not biased due to the homoscedastic nature of transcriptomic count data.

TUNEL model performance

Figure 5 shows the distributions of cross-validation and held-out test R^2 scores for the TUNEL phenotype. Again, we include the most predictive genes only from those models whose held-out test R^2 scores are 0.9 or higher and then take the genes that appear in a simple majority of those high-performing models as our final gene sets.

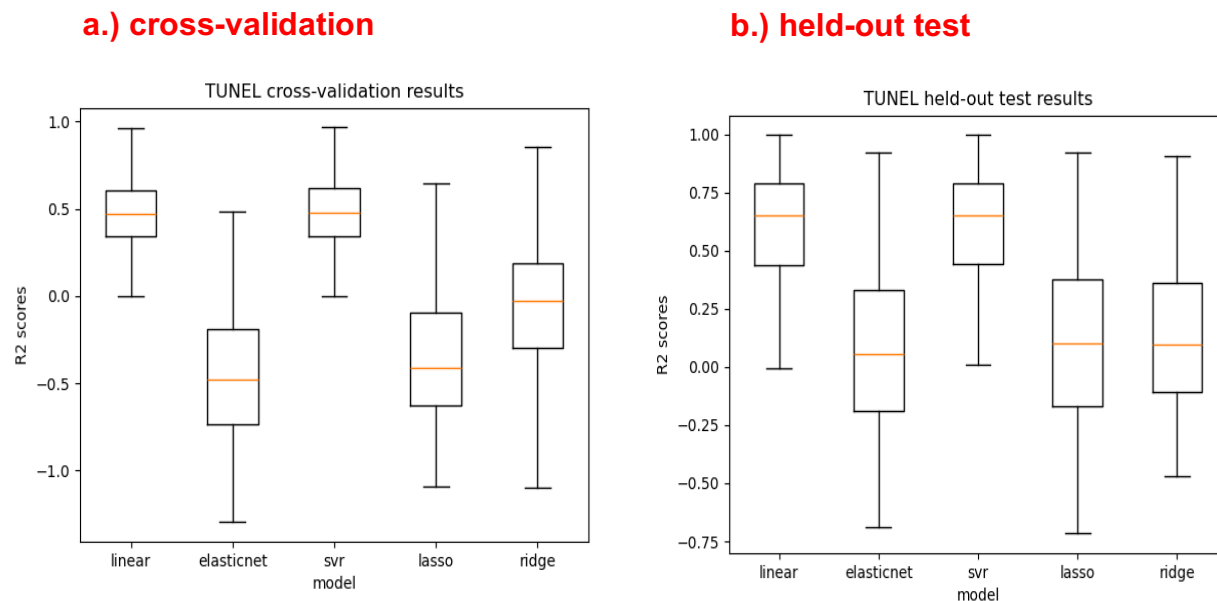## a.) cross-validation

b.) held-out test

Figure 5. Performance results from the a.) cross-validation set and b.) held-out test set for each regression model predicting the TUNEL phenotype value.

Similarly, in the case of TUNEL, three of the five models achieved R^2 scores higher than 0.9 (linear regression, elastic net regression, and support vector regression). In the construction of the final gene set for TUNEL, we select those genes which appear in the majority (2 or 3) of feature importance lists of these 3 algorithms. As shown in Figure A2 of the Appendix, the genes most predictive of the TUNEL phenotype values are approximately uniformly distributed across the background of all genes, demonstrating that the results are not biased due to the homoscedastic nature of transcriptomic count data.

The results of model performance metrics revealed strong predictive ability on both 4-HNE and TUNEL phenotypes. The linear regression and support vector regression models consistently outperformed the other models on both cross-validation and held-out test sets and have similar results to each other. The elastic net and lasso models consistently performed the worst across the datasets and have similar results to each other. The ridge regression model performance was approximately average across all 5 algorithms and both cross-validation and held-out test datasets. These results suggest our models are not overfit (the cross-validation and held-out test scores are similar), and that our sample size is likely adequate relative to the number of features we're using, though caution is still warranted due to our small sample size of n=16. The fact that our unregularized linear regression model outperforms the regularized models (lasso, ridge, elastic net) suggests that we may be over-penalizing those regularized models for their complexity (though we used grid search to identify the optimal value for the alpha regularization parameter). This in turn suggests that most genes in the feature space are informative, validating our choices in the filtering preprocessing step.

Genes uniquely predictive of the 4-HNE oxidative stress phenotype

All genes in the majority of high-performing models identified as most predictive of the 4-HNE oxidative stress phenotype are shown in Table 2. Positive average coefficient values indicate a positive correlation with the HNE target, and negative average coefficient values indicate a negative correlation with the HNE target.

Anp32a Arl6ip1 Atf4 B2m Chgb Cnga1 Cox7b Cplx1 Efemp1 Gpnmb Hint1 Hnrnpa2b1 Hnrnph1 Hsp90ab1 Hspb6 Ldhb Mrpl34 mt-Nd1 Nr2e3 Pcare Selenow Snap25 Sncb Syn1 Trf Uqcr10 Vsnl1

Table 2. Union of sets of most predictive genes from the majority of high-performing models in predicting 4-HNE listed in alphabetical order.

Table 3 shows the functional enrichment of these genes in gene sets from KEGG and Gene Ontology databases. The final gene sets associated with predicting the 4-HNE phenotype involve a complex stress response encompassing structural and morphological abnormalities (e.g. optic disc pallor), photoreceptor and retinal degeneration (e.g. retinal dystrophy), and fundamental cellular processes (e.g. neuron projection). Together, this demonstrates that 4-HNE acts as a molecular bridge connecting oxidative stress to the structural and functional pathologies observed in SANS.

Gene set name (total number of genes)	description	genes in overlap	FDR q-value
HP_OPTIC_DISC_PALLOR (257)	Optic disc pallor	*Cnga1 mt-Nd1 Pcare Nr2e3 Cox7b Efemp1 Hnrnph1*	3.06e-06
HP_OPHTHALMOPARESIS (305)	Ophthalmoparesis	*Cnga1 mt-Nd1 Pcare Nr2e3 Snap25 Hnrnpa2b1*	2.12e-04
HP_ABNORMALITY_OF_RETINAL_PIGMENTATION (332)	Abnormality of retinal pigmentation	*Cnga1 mt-Nd1 Pcare Nr2e3 Cox7b Efemp1*	2.12e-04

HP_ABNORMAL_OPTIC_NERVE_MORPHOLOGY (909)	Abnormal optic nerve morphology	*Cnga1* *mt-Nd1* *Pcare* *Nr2e3* *Cox7b* *Efemp1* *Hnrnph1* *Cplx1*	2.12e-04
GOCC_NEURON_PROJECTION (1353)	A prolongation of process extending from a nerve cell (e.g. an exon or dendrite)	*Cnga1* *mt-Nd1* *Pcare* *Snap25* *Cplx1* *Atf4* *Syn1* *Hsp90ab1* *Sncb*	2.12e-04
HP_RETINAL_DYSTROPHY (366)	Retinal dystrophy	*Cnga1* *mt-Nd1* *Pcare* *Nr2e3* *Cox7b* *Efemp1*	2.12e-04
GOCC_MEMBRANE_PROTEIN_COMPLEX (1399)	Any protein complex that is part of a membrane	*Cnga1* *mt-Nd1* *Cox7b* *Snap25* *Cplx1* *B2m* *Uqcr10* *Tf* *Arl6ip1*	2.12e-04
HP_GLAUCOMA (377)	Glaucoma	*Cnga1* *Pcare* *Nr2e3* *Cox7b* *Efemp1* *Cplx1*	2.12e-04
HP_PIGMENTARY_RETINOPATHY (212)	Pigmentary retinopathy	*Cnga1* *mt-Nd1* *Pcare* *Nr2e3*	3.36e-04

		Cox7b	
GOBP_MONOATOMIC_CATION_TRANSPORT (1079)	The directed movement of a monoatomic cation, into, out of, or within a cell, or between cells by means of some agent such as a transporter or pore.	*Cnga1* *mt-Nd1* *Cox7b* *Snap25* *B2m* *Uqcr10* *Tf*	3.36e-04

Table 3 shows the top 10 pathways and gene sets significantly enriched by the genes most predictive of HNE oxidative stress phenotype, using KEGG and Gene Ontology databases.

Comparison to results from CRISP ensemble for 4-HNE

Because CRISP is a binary classifier, we binned the HNE phenotype values as "low" and "high" based on their being lower or higher than the median HNE value, respectively. The top 20 genes most predictive of the HNE phenotype according to the CRISP ensemble that were also identified by our approach include *Hsp90ab1* and *mt-Nd1*. Moreover, when submitting the 20 CRISP genes to MSigDB, the gene sets that intersect with those enriched by our approach include GOCC_NEURON_PROJECTION and HP_OPTIC_DISC_PALLOR.

Genes uniquely predictive of the TUNEL apoptosis phenotype

All genes in the majority of high-performing models identified as most predictive of the TUNEL apoptosis phenotype are shown in Table 4.

Ddit4 Gabarapl1 Ip6k2 Mgarp Nrl Pdzph1 Reep6 Rom1 Slc24a1 Tcf20 Vtn

Table 4. Union of sets of most predictive genes from the majority of high-performing models in predicting TUNEL listed in alphabetical order.

The top genes most predictive of the TUNEL apoptosis phenotype significantly enrich the gene sets listed in Table 5. These pathways contain genes involved in photoreceptor-specific cell death (e.g. nyctalopia), structural deterioration from cell loss (e.g. retinal atrophy), and electrophysiological dysfunction (e.g. abnormal visual electrophysiology). Unlike 4-HNE's functional disruption of existing cellular machinery, TUNEL-positive signatures indicate the irreversible cellular commitment to cell death that characterize advanced stages of SANS pathology.

Gene set name (total number of genes)	description	genes in overlap	FDR q-value
HP_ATTENUATION_OF_RETINAL_BLOOD_VESSELS (141)	Attenuation of retinal blood vessels	*Rom1* *Reep6* *Nrl* *Slc24a1*	3.6e-04

HP_ABNORMAL_FULL_FIELD_ELECTRORETIN OGRAM (150)	Abnormal full-field electroretinogram	*Rom1* *Reep6* *Nrl* *Slc24a1*	3.6e-04
HP_RETINAL_ATROPHY (170)	Retinal atrophy	*Rom1* *Reep6* *Nrl* *Slc24a1*	3.97e-04
HP_PIGMENTARY_RETINOPATHY (212)	Pigmentary retinopathy	*Rom1* *Reep6* *Nrl* *Slc24a1*	4.9e-04
HP_COLOR_VISION_DEFECT (218)	Color vision defect	*Rom1* *Reep6* *Nrl* *Slc24a1*	4.9e-04
HP_NYCTALOPIA (225)	Nyctalopia	*Rom1* *Reep6* *Nrl* *Slc24a1*	4.9e-04
GOBP_SENSORY_PERCEPTION_OF_LIGHT_STI MULUS (227)	The series of events required for an organism to receive a sensory light stimulus, convert it to an electrical signal, and recognize and characterize the signal.This is a neurological process.	*Rom1* *Reep6* *Nrl* *Slc24a1*	4.9e-04
HP_ABNORMAL_ELECTRORETINOGRAM (229)	Abnormal electroretinogram	*Rom1* *Reep6* *Nrl* *Slc24a1*	4.9e-04
HP_ABNORMAL_MACULAR_MORPHOLOGY (259)	Abnormal macular morphology	*Rom1* *Reep6* *Nrl* *Slc24a1*	7.13e-04
HP_ABNORMAL_VISUAL_ELECTROPHYSIOLOG Y (275)	Abnormal visual electrophysiology	*Rom1* *Reep6* *Nrl*	7.84e-04

		Slc24a1	

Table 5 shows the top 10 pathways and gene sets significantly enriched by the genes most predictive of TUNEL apoptosis phenotype, using KEGG and Gene Ontology databases.

Comparison to results from CRISP ensemble for TUNEL

Because CRISP is a binary classifier, we binned the TUNEL phenotype values as "low" and "high" based on their being lower or higher than the median TUNEL value, respectively. The top 20 genes most predictive of the TUNEL phenotype according to the CRISP ensemble that were also identified by our approach include *Mgarp*, *Nrl*, *Reep6*, *Slc24a1*, and *Vtn*. Moreover, when submitting the 20 CRISP genes to MSigDB, the gene sets that intersect with those enriched by our approach include GOBP_SENSORY_PERCEPTION_OF_LIGHT_STIMULUS, HP_ABNORMAL_FULL_FIELD_ELECTRORETINOGRAM, HP_ABNORMAL_MACULAR_MORPHOLOGY, HP_ABNORMAL_VISUAL_ELECTROPHYSIOLOGY, and HP_ATTENUATION_OF_RETINAL_BLOOD_VESSELS.

Discussion

In this section, we discuss the results from the 4-HNE experiments and the TUNEL experiments. We consider the limitations of our approach, and we conclude with future directions for this line of research.

4-HNE Genes and Pathways

Analysis of top predictive genes for the 4-HNE phenotype (Table 2) focused on enriched Gene Ontology pathways from MSigDB C5 libraries associated with ocular pathology and function: optic disc pallor, ophthalmoparesis, retinal pigmentation abnormalities, abnormal optic nerve morphology, neuron projection, retinal dystrophy, membrane protein complex, glaucoma, pigmentary retinopathy, and monoatomic cation pathways. This approach identified *B2m*, *Uqcr10*, *Tf*, *Arl6ip1*, *Cnga1*, *Mt-nd1*, *Pcare*, *Hnrnph1*, *Snap25*, *Hnrnpa2b1*, *Cplx1*, *Atf4*, *Syn1*, *Hsp90ab1*, *Sncb*, *Nr2e3*, *Cox7b*, and *Efemp1* as genes linked to pathways and pathologies paralleling SANS symptoms.

Genes *B2m*, *Tf*, *Arl6ip1*, and *Uqcr10* converge on membrane-associated pathways (GO:0098796). Upregulated *B2m* reflects heightened immune signaling following oxidative injury [32]. *Tf* expression changes suggest altered iron homeostasis under oxidative stress [33]. *Arl6ip1*, an apoptotic regulator, supports adaptive responses to endoplasmic reticulum and membrane stress through mitochondria-associated membrane localization [34]. Elevated *Uqcr10* reflects compensatory mitochondrial remodeling since 4-HNE disrupts respiratory-chain proteins [35].

4-HNE modifies essential photoreceptor proteins (*Cnga1*, *Mt-Nd1*, *Pcare*) contributing to retinal degeneration. *Cnga1* encodes the rod cGMP-gated ion channel, and HNE binding disrupts cation flow and signal conversion [36]. *Mt-Nd1* modification reduces ATP production and elevates ROS [37], whereas disruption of *Pcare* impairs photoreceptor disc organization [38].

Hnrnph1 enrichment indicates 4-HNE affects RNA processing that supports retinal and optic nerve function [39]. *Snap25* enrichment reflects synaptic protein susceptibility to lipid peroxidation [40]. Its appearance in ophthalmoparesis phenotypes indicates disrupted neuromuscular signaling [41]. *Cplx1* enrichment suggests synaptic release alterations contribute to optic nerve deterioration [42].

Efemp1 dysregulation causes Doyne honeycomb retinal dystrophy, myopia, glaucoma, and drusen accumulation [43]. Spaceflight-disrupted integrin signaling affects retinal vascular permeability, while microgravity-induced collagen stretching [44] potentially causes SANS eye deformation. 4-HNE directly impacts ERK levels [45], increasing cell stress.

Atf4, *Syn1*, *Hsp90Ab1*, and *Sncb* demonstrate functional relationships within 4-HNE exposure relating to neuron projection (GO:0043005) and monoatomic cation transport. *Atf4* regulates vascular associated cell apoptotic processes [46], while *Hsp90Ab1* refolds damaged proteins to prevent endoplasmic reticulum stress-induced apoptosis [47]. At synaptic terminals, 4-HNE alters *Syn1* phosphorylation (which disrupts vesicle tethering) [48], while *Sncb* modification promotes oxidative stress and inflammatory response [49]. Chronic HNE elevation overwhelms protective capacity, causing synaptic dysfunction.

TUNEL Genes and Pathways

For TUNEL, the focus differs substantially from 4-HNE. Endothelial dysfunction is highly relevant to ocular dysfunction. The corneal endothelium is critical for corneal homeostasis, and Zanello et al. found corneal bullae in spaceflown mice [50]. Endothelial dysfunction in retinal vasculature causes retinal insufficiency, possibly linking to cotton wool spots seen in astronauts, consistent with blood-retinal barrier disruption and ocular adaptations documented in RR-9 mission samples [11]. Analysis of the TUNEL phenotype highlighted key predictive genes: *Ddit4*, *Nrl*, *Tcf20*, *Pdzph1*, *Gabarapl1*, *Ip6k2*, *Mgarp*, *Reep6*, *Rom1*, *Slc24a1*, and *Vtn*. Gene set enrichment showed association with apoptotic signaling, photoreceptor cell death, structural deterioration, and retinopathy pathways. This is consistent with the fact that TUNEL specifically detects DNA fragmentation indicating apoptosis.

Ddit4 (also known as *Redd1*) participates in regulating stress-induced apoptosis through mTORC1 inhibition and ROS control, with *Ddit4* knockdown preserving cell viability and inhibiting apoptosis under hyperosmolarity [51]. Upregulation of *Ddit4* expression in response to cellular stress activates autophagy and apoptosis through the mTOR signaling axis, particularly in differentiated cells exposed to neurotoxic insults [52]. *Ddit4* acts as a negative regulator of mTOR in response to hypoxia, DNA damage, and energy stress [53,54], with clinical significance related to aging-associated diseases [55]. These pathways directly parallel microgravity-induced stress responses in spaceflight conditions.

Nrl is critical for rod photoreceptor cell differentiation and homeostasis, with *Nrl* mutations leading to loss of rods and increased cone populations, and inhibition of *Nrl* activity preventing cell death in multiple retinal degeneration models [56]. *Nrl* regulates rod-specific genes including *Rom1*, *Samd7*, *Nr2e3*, *Cngb1*, and *Pde6g*, essential for proper photoreceptor identity and survival [57]. *Rom1* regulates outer segment disc formation in association with *Prph2*, with *Rom1* disruption causing slow photoreceptor degeneration and outer nuclear layer thinning [58], reflecting cell types typically more vulnerable in SANS. These findings align with direct

experimental observations of spaceflight-induced photoreceptor dysfunction and retinal functional impairment in mice [7].

Reep6 is critical for rod photoreceptor endoplasmic reticulum homeostasis and trafficking of essential phototransduction proteins, with *Reep6* deficiency causing early onset photoreceptor dysfunction preceding degeneration through ER stress induction [59]. *Reep6* knockout mice exhibit progressive photoreceptor degeneration with altered subcellular localization of phototransduction proteins, including impaired trafficking of retinal guanylate cyclases GC1 and GC2 [59]. *Rom1* is required for rod photoreceptor viability and the regulation of disk morphogenesis [60], while *Pde6g* encodes the inhibitory γ subunit of rod cGMP-phosphodiesterase essential for maintaining phototransduction cascade function [61]. Dysregulation of either contributes to photoreceptor degeneration.

Gabarapl1, a member of the GABARAP subfamily essential for autophagosome-lysosome fusion [62], shows significantly elevated expression in retinal pigment epithelial cells under oxidative stress [63]. *Gabarapl1* shows dual protective roles during acute oxidative stress through enhanced autophagic flux, while chronic elevation may transition to pathological autophagy [64], demonstrating context-dependent regulation critical for managing cellular debris and maintaining retinal structural integrity during prolonged microgravity exposure. *Tcf20* was originally identified by its ability to bind the stromelysin-1 PDGF-responsive element [65] and subsequently characterized as a transcriptional coactivator that enhances the activity of multiple transcription factors with widespread tissue expression [66]. *Pdzph1* (PDZ and pleckstrin homology domains 1), identified as predictive of the TUNEL phenotype, encodes a protein containing PDZ and pleckstrin homology domains. While its specific function in photoreceptors remains uncharacterized, PDZ domain proteins are known to regulate synaptic organization and photoreceptor-bipolar cell connections [67], suggesting that TUNEL-positive signals may reflect compromised protein trafficking or synaptic integrity.

The *Vtn* gene encodes vitronectin, an extracellular matrix glycoprotein detected in photoreceptors, Bruch's membrane, and retinal vasculature that promotes cell adhesion and spreading through integrin-RGD interactions [68]. *Vtn* promotes retinal neurite outgrowth and is upregulated following retinal injury [69], and reduced vitronectin expression could impair photoreceptor-epithelial interactions vulnerable to spaceflight stress. *Mgarp* (mitochondria-localized glutamic acid-rich protein), highly expressed in retinal photoreceptor inner segments [70], regulates mitochondrial transport and distribution, particularly under hypoxic stress conditions [71]. Reduced *Mgarp* expression may compromise mitochondrial trafficking to photoreceptor terminals during spaceflight stress.

Conclusion

This machine learning ensemble identified distinct genes predictive of 4-HNE-mediated oxidative damage and TUNEL-positive apoptosis in spaceflown murine retinae. For the 4-HNE phenotype, predictive genes converged on membrane-associated pathways, photoreceptor protein modification, synaptic dysfunction, and extracellular matrix dysregulation, with key contributors including *B2m*, *Tf*, *Cnga1*, *mt-Nd1*, *Snap25*, and *Efemp1* reflecting oxidative stress-induced damage to critical ocular structures. The TUNEL phenotype revealed a distinct signature emphasizing stress-induced apoptosis, photoreceptor degeneration, and endoplasmic reticulum dysfunction, with *Ddit4*, *Nrl*, *Rom1*, *Reep6*, and *Gabarapl1* emerging as central regulators of cell

death pathways particularly relevant to rod photoreceptor vulnerability. Together, these findings demonstrate that oxidative lipid peroxidation and apoptotic cell death may represent complementary pathological mechanisms in SANS. This molecular framework provides potential noninvasive biomarkers for monitoring spaceflight-induced neuro-ocular changes and suggests therapeutic targets for protecting astronaut visual health during long-duration missions. As humanity extends its presence beyond low Earth orbit, such molecular insights and translational strategies will prove essential for safeguarding crew health and mission success during deep-space exploration.

Strengths and Limitations

4-HNE staining visually shows tissue concentration, serving as a preferred tool for detecting spaceflight stresses as a direct lipid peroxidation indicator. 4-HNE adducts are more stable than ROS, making post-flight analysis easier given sample transport delays. Immunostaining allows localized tissue visualization. Limitations include 4-HNE not being SANS-specific, potential cross-reactivity concerns, and inter-laboratory variability in ELISA sensitivities [72]. Uncertainty exists regarding 4-HNE adduct detection timing after spaceflight exposure.

The TUNEL assay provides sensitive histological readout on DNA fragmentation associated with apoptotic cell death. Strengths include relative technical simplicity, standardized commercial kit availability, and ability to spatially localize cell death within vulnerable retinal layers including GCL, INL, and photoreceptors [73]. However, DNA strand breaks are labeled regardless of underlying cause, and the assay cannot reliably distinguish apoptosis from necrosis, autolysis, DNA repair, or irradiation-induced damage [74]. TUNEL primarily reflects late-stage cell death endpoints with limited insight into upstream molecular triggers. Sensitivity varies with tissue handling and timing [75], a consideration particularly relevant for spaceflight biological studies where post-flight processing delays are common and could increase the likelihood of false negatives. When interpreted with complementary markers, TUNEL remains powerful for assessing cumulative retinal damage in preclinical SANS studies.

Our computational approach has several limitations. The small sample size (n=16) increases vulnerability to individual sample variability. The identified genes represent machine-learned associations rather than confirmed causal mechanisms. Without functional validation, we cannot definitively establish whether modulating these genes would alter 4-HNE or TUNEL phenotypes. Bulk RNA-sequencing provides only a single temporal snapshot and does not capture acute molecular changes during spaceflight or recovery trajectory. Bulk tissue analysis averages expression across heterogeneous cell populations, masking cell-type-specific responses critical to SANS pathogenesis. Gene filtering likely discarded regulatory RNAs, low-abundance transcription factors, or genes with nonlinear phenotype relationships that may play important mechanistic roles.

Future Directions

While this study establishes transcriptomic signatures predictive of oxidative stress and apoptosis in spaceflight-exposed retinal tissue, several key steps are needed to validate and extend these findings. The identified genes require experimental validation through both *in vitro* and *in vivo* approaches, including retinal cell lines exposed to radiation or oxidative stressors, or transgenic mice during simulated spaceflight. Future research requires temporal profiling with multiple

sampling timepoints (preflight, during flight, post-flight, and extended recovery) to capture molecular response dynamics, following the paradigm established by the NASA Twins Study [76]. Single-cell and spatial transcriptomics would resolve cell-type-specific vulnerabilities [77], potentially revealing distinct molecular responses in photoreceptors, endothelial cells, and ganglion cells. Expanded sample sizes across multiple missions would strengthen statistical confidence. Human ground-based analogs such as head-down tilt bed rest [78], dry immersion [79] and prospective astronaut studies with accessible biospecimens (tears, blood) or imaging biomarkers would establish clinical relevance. Research on extended reality quantification of pupil reactivity identified pupillometry as a promising non-invasive biomarker for detecting elevated intracranial pressure changes during spaceflight [80]. Several researchers have also contributed to investigations of the spaceflight contrast sensitivity hypothesis, evaluating how visual dysfunction relates to SANS pathophysiology through novel visual assessment technologies [81].

More broadly, this study exemplifies an emerging paradigm in which machine learning approaches extract predictive insights from existing spaceflight datasets - an approach that will become increasingly critical as deep-space missions exceed the duration and distance where real-time Earth-based medical support is feasible. Recent frameworks have outlined how artificial intelligence can enable autonomous biomonitoring and precision health during extended missions [82], as well as support automated science and self-driving laboratory capabilities for biological research beyond low Earth orbit where crew time is precious [83]. The ensemble methodology demonstrated here represents one component of this larger vision: systematically mining NASA's data as well as data from academic, commercial, and international sources to generate actionable biological insights that inform crew health monitoring, countermeasure development, and mission planning for lunar and Martian exploration.

Acknowledgements

Funding

Data and Code Availability

All experimental data used in this study are publicly available through NASA's Open Science Data Repository, the expansion of NASA GeneLab to integrate the NASA Ames Life Sciences Data Archive to include high quality physiological, phenotypic, bioimaging, environmental telemetry, and behavior (https://science.nasa.gov/biological-physical/data/osdr/). The three Rodent Research 9 (RR-9) mission datasets were mined from: 1) OSD-255 containing retinal RNA sequencing gene expression data (https://doi.org/10.26030/mebr-1747), 2) OSD-557 containing 4-HNE immunostaining microscopy data for oxidative stress quantification (https://doi.org/10.26030/yv31-1a54), and 3) OSD-568 containing TUNEL assay microscopy data for apoptosis detection (https://doi.org/10.26030/d09k-4e68). Gene set enrichment analyses were performed using the Molecular Signatures Database (MSigDB; https://www.gsea-msigdb.org/gsea/msigdb). All Python code for data preprocessing, machine learning model training, feature selection, and visualization is available at https://colab.research.google.com/drive/11moJztlWNqPYNUfef6Ids9mOl1xmpSXb?usp=sharing.

Authors' Contributions

LMS, JAC, RTS, and PAV were co-investigators in the grant described in the Funding section. This grant led to the design and development of an online training course in which high school students learned how to use artificial intelligence and machine learning to study the effect of spaceflight on living systems. JAC designed and implemented the Jupyter notebooks for that course to analyze the molecular retina data from the RR9 mission. The students in that course wrote reports based on the results of these analyses. JAC developed the first version of this manuscript by integrating components from the reports of the students who expressed interest in participating in this research (AR, Aarav J, AC, AA, AP, AN, Anishka J, AB, AK, Anagha J, BP, DS, DN, EK, EP, FPU, IS, IY, JW, JL, KS, MPDM, MH, ML, MV, Misha K, Mrinalini K, MAJ, MA, NZC, NA, NBC, RH, RP, SD, Samarth S, Shawnak S, SG, Shriya S, SC, VP, VN, and ZS). PP and JC organized the efforts of the students. DMT and AL ran the CRISP experiments. The biomedical experts (JO, XWM, EW, and LMS) provided feedback and guidance for revising the first version of the manuscript. RTS and JAC wrote the final version of the manuscript based on that feedback. PAV, SG, and JMG provided management oversight and support of the research. All authors proofread the manuscript and provided their feedback.

Conflicts of Interest

The other authors declare no competing interests.

References

1. Afshinnekoo E, Scott RT, MacKay MJ, Pariset E, Cekanaviciute E, Barker R, et al. Fundamental biological features of spaceflight: advancing the field to enable deep-space exploration. Cell. Nov 25, 2020;183(5):1162-1184. [doi: 10.1016/j.cell.2020.10.050] [Medline: 33242416]

2. Mader TH, Gibson CR, Pass AF, Kramer LA, Lee AG, Fogarty J, et al. Optic disc edema, globe flattening, choroidal folds, and hyperopic shifts observed in astronauts after long-duration space flight. Ophthalmology. Oct 2011;118(10):2058-2069. [doi: 10.1016/j.ophtha.2011.06.021] [Medline: 21849212]

3. Mao XW, Pecaut MJ, Stodieck LS, Ferguson VL, Bateman TA, Bouxsein M, et al. Spaceflight environment induces mitochondrial oxidative damage in ocular tissue. Radiat Res. Oct 2013;180(4):340-350. [doi: 10.1667/RR3309.1] [Medline: 24033191]

4. Lee AG, Mader TH, Gibson CR, Tarver W, Rabiei P, Riascos RF, et al. Spaceflight associated neuro-ocular syndrome (SANS) and the neuro-ophthalmologic effects of microgravity: a review and an update. NPJ Microgravity. Feb 7, 2020;6:7. [doi: 10.1038/s41526-020-0097-9] [Medline: 32047839]

5. Nelson ES, Mulugeta L, Myers JG. Microgravity-induced fluid shift and ophthalmic changes. Life (Basel). Nov 7, 2014;4(4):621-665. [doi: 10.3390/life4040621] [Medline: 25387162]

6. Verma A, Bacci T, Sarraf D, Freund KB, Sadda SR. Vortex vein imaging: what can it tell us? Clin Ophthalmol. Aug 10, 2021;15:3321-3331. [doi: 10.2147/OPTH.S324075] [Medline: 34408390]

7. Mao X, Stanbouly S, Holley J, Pecaut M, Crapo J. Evidence of spaceflight-induced adverse effects on photoreceptors and retinal function in the mouse eye. Int J Mol Sci. Apr 17, 2023;24(8):7362. [doi: 10.3390/ijms24087362] [Medline: 37108526]

8. Kyrylkova K, Kyryachenko S, Leid M, Kioussi C. Detection of apoptosis by TUNEL assay. Methods Mol Biol. 2012;887:41-47. [doi: 10.1007/978-1-61779-860-3_5] [Medline: 22566045]

9. Overbey EG, da Silveira WA, Stanbouly S, Nishiyama NC, Roque-Torres GD, Pecaut MJ, et al. Spaceflight influences gene expression, photoreceptor integrity, and oxidative stress-related damage in the murine retina. Sci Rep. Sep 16, 2019;9(1):13304. [doi: 10.1038/s41598-019-49453-x] [Medline: 31527661]

10. Mao XW, Byrum S, Nishiyama NC, Pecaut MJ, Sridharan V, Boerma M, et al. Impact of spaceflight and artificial gravity on the mouse retina: biochemical and proteomic analysis. Int J Mol Sci. Aug 28, 2018;19(9):2546. [doi: 10.3390/ijms19092546] [Medline: 30154332]

11. Mao XW, Nishiyama NC, Byrum SD, Stanbouly S, Jones T, Drew A, et al. Characterization of mouse ocular response to a 35-day spaceflight mission: evidence of blood-retinal barrier disruption and ocular adaptations. Sci Rep. Jun 3, 2019;9(1):8215. [doi: 10.1038/s41598-019-44696-0] [Medline: 31160660]

12. Scott RT, Grigorev K, Mackintosh G, Gebre SG, Mason CE, Del Alto ME, et al. Advancing the integration of biosciences data sharing to further enable space exploration. Cell Rep. Dec 8, 2020;33(10):108441. [doi: 10.1016/j.celrep.2020.108441] [Medline: 33242404]

13. Gebre SG, Scott RT, Saravia-Butler AM, Lopez DK, Sanders LM, Costes SV. NASA Open Science Data Repository: open science for life in space. Nucleic Acids Res. Jan 6, 2025;53(D1):D1697-D1710. [doi: 10.1093/nar/gkae1116] [Medline: 39558178]

14. Overbey EG, da Silveira WA, Stanbouly S, Nishiyama NC, Roque-Torres GD, Pecaut MJ, et al. Spaceflight influences gene expression, photoreceptor integrity, and oxidative stress related damage

in the murine retina (RR-9). NASA Ames Life Sciences Data Archive. OSD-557, v3, 2023. [doi: 10.26030/yv31-1a54]

15. Xiao M, Nishiyama NC, Byrum SD, Stanbouly S, Jones T, Drew A, et al. Characterization of mouse ocular responses (microscopy) to a 35-day (RR-9) spaceflight mission: evidence of blood-retinal barrier disruption and ocular adaptations. NASA Ames Life Sciences Data Archive. OSD-568, v3, 2024. [doi: 10.26030/D09K-4E68]

16. Mao XW. Spaceflight influences gene expression, photoreceptor integrity, and oxidative stress-related damage in the murine retina. NASA GeneLab. OSD-255, v5, 2024. [doi: 10.26030/MEBR-1747]

17. Li B, Dewey CN. RSEM: accurate transcript quantification from RNA-Seq data with or without a reference genome. BMC Bioinformatics. Aug 4, 2011;12:323. [doi: 10.1186/1471-2105-12-323] [Medline: 21816040]

18. Dobin A, Davis CA, Schlesinger F, Drenkow J, Zaleski C, Jha S, et al. STAR: ultrafast universal RNA-seq aligner. Bioinformatics. Jan 1, 2013;29(1):15-21. [doi: 10.1093/bioinformatics/bts635] [Medline: 23104886]

19. GeneLab_Data_Processing: standard bioinformatics pipelines for omics data from spaceflight and space-relevant experiments. Github. URL: https://github.com/nasa/GeneLab_Data_Processing/tree/master [Accessed Jan 16, 2026]

20. Overbey EG, Saravia-Butler AM, Zhang Z, Rathi KS, Fogle H, da Silveira WA, et al. NASA GeneLab RNA-seq consensus pipeline: standardized processing of short-read RNA-seq data. iScience. Apr 23, 2021;24(4):102361. [doi: 10.1016/j.isci.2021.102361] [Medline: 33870146]

21. Casaletto JA, Zhao T, Yeung J, Lee A, Ansari A, Fry A, et al. Machine learning ensemble investigates age in the transcriptomic response to spaceflight in murine mammary tissue: observational study. JMIRx Bio. Jan 14, 2026;4:e73041. [doi: 10.2196/73041]

22. Maulud D, Abdulazeez AM. A review on linear regression comprehensive in machine learning. J Appl Sci Technol Trends. Dec 31, 2020;1(2):140-147. [doi: 10.38094/jastt1457]

23. Cervantes J, Garcia-Lamont F, Rodríguez-Mazahua L, Lopez A. A comprehensive survey on support vector machine classification: applications, challenges and trends. Neurocomputing. Sep 2020;408:189-215. [doi: 10.1016/j.neucom.2019.10.118]

24. Dupré la Tour T, Eickenberg M, Nunez-Elizalde AO, Gallant JL. Feature-space selection with banded ridge regression. Neuroimage. Dec 1, 2022;264:119728. [doi: 10.1016/j.neuroimage.2022.119728] [Medline: 36334814]

25. Muthukrishnan R, Rohini R. LASSO: a feature selection technique in predictive modeling for machine learning. Presented at: 2016 IEEE International Conference on Advances in Computer Applications (ICACA); Oct 24, 2016; Coimbatore, India. [doi: 10.1109/icaca.2016.7887916]

26. Ogutu JO, Schulz-Streeck T, Piepho HP. Genomic selection using regularized linear regression models: ridge regression, lasso, elastic net and their extensions. BMC Proc. May 21, 2012;6(Suppl 2):S10. [doi: 10.1186/1753-6561-6-S2-S10] [Medline: 22640436]

27. Wong TT, Yeh PY. Reliable accuracy estimates from k-fold cross validation. IEEE Trans Knowl Data Eng. Aug 1, 2020;32(8):1586-1594. [doi: 10.1109/tkde.2019.2912815]

28. Altmann A, Toloşi L, Sander O, Lengauer T. Permutation importance: a corrected feature importance measure. Bioinformatics. May 15, 2010;26(10):1340-1347. [doi: 10.1093/bioinformatics/btq134] [Medline: 20385727]

29. Guyon I, Weston J, Barnhill S, Vapnik V. Gene selection for cancer classification using support vector machines. Mach Learn. Jan 2002;46(1-3):389-422. [doi: 10.1023/A:1012487302797]

30. Subramanian A, Tamayo P, Mootha VK, Mukherjee S, Ebert BL, Gillette MA, et al. Gene set enrichment analysis: a knowledge-based approach for interpreting genome-wide expression profiles. Proc Natl Acad Sci U S A. Oct 25, 2005;102(43):15545-15550. [doi: 10.1073/pnas.0506580102] [Medline: 16199517]

31. Casaletto JA, Scott RT, Myrick M, Mackintosh G, Chok H, Saravia-Butler A, et al. Analyzing the relationship between gene expression and phenotype in space-flown mice using a causal inference machine learning ensemble. Sci Rep. Jan 18, 2025;15(1):2363. [doi: 10.1038/s41598-024-81394-y] [Medline: 39824847]

32. Yuan M, Hu X, Xing W, Wu X, Pu C, Guo W, et al. B2M is a biomarker associated with immune infiltration in high altitude pulmonary edema. Comb Chem High Throughput Screen. 2024;27(1):168-185. [doi: 10.2174/1386207326666230510095840] [Medline: 37165489]

33. Meneghini R. Iron homeostasis, oxidative stress, and DNA damage. Free Radic Biol Med. 1997;23(5):783-792. [doi: 10.1016/S0891-5849(97)00016-6] [Medline: 9296456]

34. Bishayee K, Habib K, Nazim UM, Kang J, Szabo A, Huh SO, et al. RNA binding protein HuD promotes autophagy and tumor stress survival by suppressing mTORC1 activity and augmenting ARL6IP1 levels. J Exp Clin Cancer Res. Jan 10, 2022;41(1):18. [doi: 10.1186/s13046-021-02203-2] [Medline: 35012594]

35. Sun W, Shangguan Z, Li J, Ye X, Lin Q, Chen G. UQCR10 and TNNT1: novel biomarkers for sarcopenia identified through integrated transcriptomic analysis and machine learning. Eur J Med Res. Dec 1, 2025;30(1):1197. [doi: 10.1186/s40001-025-03471-w] [Medline: 41320776]

36. Xue J, Han Y, Zeng W, Wang Y, Jiang Y. Structural mechanisms of gating and selectivity of human rod CNGA1 channel. Neuron. Apr 21, 2021;109(8):1302-1313.e4. [doi: 10.1016/j.neuron.2021.02.007] [Medline: 33651975]

37. Lin X, Zhou Y, Xue L. Mitochondrial complex I subunit MT-ND1 mutations affect disease progression. Heliyon. Apr 15, 2024;10(7):e28808. [doi: 10.1016/j.heliyon.2024.e28808] [Medline: 38596130]

38. Corral-Serrano JC, Messchaert M, Dona M, Peters TA, Kamminga LM, van Wijk E, et al. C2orf71a/pcare1 is important for photoreceptor outer segment morphogenesis and visual function in zebrafish. Sci Rep. Jun 26, 2018;8(1):9675. [doi: 10.1038/s41598-018-27928-7] [Medline: 29946172]

39. Kim GH, Kwon I. Distinct roles of hnRNPH1 low-complexity domains in splicing and transcription. Proc Natl Acad Sci U S A. Dec 14, 2021;118(50):e2109668118. [doi: 10.1073/pnas.2109668118] [Medline: 34873036]

40. Zhang C, Xie S, Malek M. SNAP-25: a biomarker of synaptic loss in neurodegeneration. Clin Chim Acta. Apr 15, 2025;571:120236. [doi: 10.1016/j.cca.2025.120236] [Medline: 40058720]

41. Keene KR, Kan HE, van der Meeren S, Verbist BM, Tannemaat MR, Beenakker JWM, et al. Clinical and imaging clues to the diagnosis and follow-up of ptosis and ophthalmoparesis. J Cachexia Sarcopenia Muscle. Dec 2022;13(6):2820-2834. [doi: 10.1002/jcsm.13089] [Medline: 36172973]

42. Chang S, Reim K, Pedersen M, Neher E, Brose N, Taschenberger H. Complexin stabilizes newly primed synaptic vesicles and prevents their premature fusion at the mouse calyx of held synapse. J Neurosci. May 27, 2015;35(21):8272-8290. [doi: 10.1523/JNEUROSCI.4841-14.2015] [Medline: 26019341]

43. Wood AJ, Livingstone I, Westcott M, Furniss D, Wiberg A. A review of the role of EFEMP1 in ophthalmic disease. Ophthalmic Genet. 2025;46(6):523-531. [doi: 10.1080/13816810.2025.2524511] [Medline: 40640104]

44. Solano MM, Dumas R, Lesk MR, Costantino S. Ocular biomechanical responses to long-duration spaceflight. IEEE Open J Eng Med Biol. 2025;6:127-132. [doi: 10.1109/ojemb.2024.3453049] [Medline: 39698125]

45. Ioannidis M, Tjepkema J, Uitbeijerse MRP, van den Bogaart G. Immunomodulatory effects of 4-hydroxynonenal. Redox Biol. Sep 2025;85:103719. [doi: 10.1016/j.redox.2025.103719] [Medline: 40489926]

46. Chen D, Fan Z, Rauh M, Buchfelder M, Eyupoglu IY, Savaskan N. ATF4 promotes angiogenesis and neuronal cell death and confers ferroptosis in a xCT-dependent manner. Oncogene. Oct 5, 2017;36(40):5593-5608. [doi: 10.1038/onc.2017.146] [Medline: 28553953]

47. Liu J, Yu H, Yu S, Liu M, Chen X, Wang Y, et al. GLCCI1 alleviates GRP78-initiated endoplasmic reticulum stress-induced apoptosis of retinal ganglion cells in diabetic retinopathy by upregulating and interacting with HSP90AB1. Sci Rep. Nov 4, 2024;14(1):26665. [doi: 10.1038/s41598-024-75874-4] [Medline: 39496608]

48. Bonanomi D, Menegon A, Miccio A, Ferrari G, Corradi A, Bhinder S, et al. Phosphorylation of synapsin I by cAMP-dependent protein kinase controls synaptic vesicle dynamics in developing neurons. J Neurosci. Aug 10, 2005;25(32):7299-7308. [doi: 10.1523/JNEUROSCI.1573-05.2005] [Medline: 16093379]

49. Hadrian K, Melkonyan H, Schlatt S, Wistuba J, Wasmuth S, Heiligenhaus A, et al. Age-related distribution and potential role of SNCB in topographically different retinal areas of the common marmoset Callithrix jacchus, including the macula. Exp Eye Res. Aug 2019;185:107676. [doi: 10.1016/j.exer.2019.05.016] [Medline: 31128101]

50. Zanello SB, Theriot CA, Ponce CMP, Chevez-Barrios P. Spaceflight effects and molecular responses in the mouse eye: preliminary observations after shuttle mission STS-133. Gravit Space Res. Jul 1, 2013;1(1):29-46. [doi: 10.2478/gsr-2013-0003]

51. Wang B, Peng L, Ouyang H, Wang L, He D, Zhong J, et al. Induction of DDIT4 impairs autophagy through oxidative stress in dry eye. Invest Ophthalmol Vis Sci. Jul 1, 2019;60(8):2836-2847. [doi: 10.1167/iovs.19-27072] [Medline: 31266058]

52. Li L, Xi L, Wu J, Zhao Z, Chen Y, Liu W, et al. The regulatory roles of DDIT4 in TDCIPP-induced autophagy and apoptosis in PC12 cells. J Environ Sci (China). Mar 2023;125:823-830. [doi: 10.1016/j.jes.2022.02.046] [Medline: 36375964]

53. Brugarolas J, Lei K, Hurley RL, Manning BD, Reiling JH, Hafen E, et al. Regulation of mTOR function in response to hypoxia by REDD1 and the TSC1/TSC2 tumor suppressor complex. Genes Dev. Dec 1, 2004;18(23):2893-2904. [doi: 10.1101/gad.1256804] [Medline: 15545625]

54. Sofer A, Lei K, Johannessen CM, Ellisen LW. Regulation of mTOR and cell growth in response to energy stress by REDD1. Mol Cell Biol. Jul 2005;25(14):5834-5845. [doi: 10.1128/MCB.25.14.5834-5845.2005] [Medline: 15988001]

55. Kim JY, Kwon YG, Kim YM. The stress-responsive protein REDD1 and its pathophysiological functions. Exp Mol Med. Sep 2023;55(9):1933-1944. [doi: 10.1038/s12276-023-01056-3] [Medline: 37653030]

56. Moore SM, Skowronska-Krawczyk D, Chao DL. Targeting of the NRL pathway as a therapeutic strategy to treat retinitis pigmentosa. J Clin Med. Jul 13, 2020;9(7):2224. [doi: 10.3390/jcm9072224] [Medline: 32668775]

57. Kallman A, Capowski EE, Wang J, Kaushik AM, Jansen AD, Edwards KL, et al. Investigating cone photoreceptor development using patient-derived NRL null retinal organoids. Commun Biol. Feb 21, 2020;3(1):82. [doi: 10.1038/s42003-020-0808-5] [Medline: 32081919]

58. Collin GB, Gogna N, Chang B, Damkham N, Pinkney J, Hyde LF, et al. Mouse models of inherited retinal degeneration with photoreceptor cell loss. Cells. Apr 10, 2020;9(4):931. [doi: 10.3390/cells9040931] [Medline: 32290105]

59. Agrawal SA, Burgoyne T, Eblimit A, Bellingham J, Parfitt DA, Lane A, et al. REEP6 deficiency leads to retinal degeneration through disruption of ER homeostasis and protein trafficking. Hum Mol Genet. Jul 15, 2017;26(14):2667-2677. [doi: 10.1093/hmg/ddx149] [Medline: 28475715]

60. Clarke G, Goldberg AF, Vidgen D, Collins L, Ploder L, Schwarz L, et al. Rom-1 is required for rod photoreceptor viability and the regulation of disk morphogenesis. Nat Genet. May 2000;25(1):67-73. [doi: 10.1038/75621] [Medline: 10802659]

61. Dvir L, Srour G, Abu-Ras R, Miller B, Shalev SA, Ben-Yosef T. Autosomal-recessive early-onset retinitis pigmentosa caused by a mutation in PDE6G, the gene encoding the gamma subunit of rod cGMP phosphodiesterase. Am J Hum Genet. Aug 13, 2010;87(2):258-264. [doi: 10.1016/j.ajhg.2010.06.016] [Medline: 20655036]

62. Nguyen TN, Padman BS, Usher J, Oorschot V, Ramm G, Lazarou M. Atg8 family LC3/GABARAP proteins are crucial for autophagosome-lysosome fusion but not autophagosome formation during PINK1/Parkin mitophagy and starvation. J Cell Biol. Dec 19, 2016;215(6):857-874. [doi: 10.1083/jcb.201607039] [Medline: 27864321]

63. Shu CW, Bee YS, Chen JL, Tsen CL, Tsai WL, Sheu SJ. Detection of autophagy-related gene expression by conjunctival impression cytology in age-related macular degeneration. Diagnostics (Basel). Feb 12, 2021;11(2):296. [doi: 10.3390/diagnostics11020296] [Medline: 33673354]

64. Kozhevnikova OS, Telegina DV, Tyumentsev MA, Kolosova NG. Disruptions of autophagy in the rat retina with age during the development of age-related-macular-degeneration-like retinopathy. Int J Mol Sci. Sep 27, 2019;20(19):4804. [doi: 10.3390/ijms20194804] [Medline: 31569675]

65. Sanz L, Moscat J, Diaz-Meco MT. Molecular characterization of a novel transcription factor that controls stromelysin expression. Mol Cell Biol. Jun 1995;15(6):3164-3170. [doi: 10.1128/MCB.15.6.3164] [Medline: 7760812]

66. Rekdal C, Sjøttem E, Johansen T. The nuclear factor SPBP contains different functional domains and stimulates the activity of various transcriptional activators. J Biol Chem. Dec 22, 2000;275(51):40288-40300. [doi: 10.1074/jbc.m006978200] [Medline: 10995766]

67. Feng W, Zhang M. Organization and dynamics of PDZ-domain-related supramodules in the postsynaptic density. Nat Rev Neurosci. Feb 2009;10(2):87-99. [doi: 10.1038/nrn2540] [Medline: 19153575]

68. Hageman GS, Mullins RF, Russell SR, Johnson LV, Anderson DH. Vitronectin is a constituent of ocular drusen and the vitronectin gene is expressed in human retinal pigmented epithelial cells. FASEB J. Mar 1999;13(3):477-484. [doi: 10.1096/fasebj.13.3.477] [Medline: 10064614]

69. Wang AG, Yen MY, Hsu WM, Fann MJ. Induction of vitronectin and integrin alphav in the retina after optic nerve injury. Mol Vis. Feb 3, 2006;12:76-84. [Medline: 16479252]

70. Qi S, Wang Y, Zhou M, Ge Y, Yan Y, Wang J, et al. A mitochondria-localized glutamic acid-rich protein (MGARP/OSAP) is highly expressed in retina that exhibits a large area of intrinsic disorder. Mol Biol Rep. Jun 2011;38(5):2869-2877. [doi: 10.1007/s11033-010-9948-x] [Medline: 20107910]

71. Li Y, Lim S, Hoffman D, Aspenstrom P, Bhinder S, Bhinder S, et al. HUMMR, a hypoxia- and HIF-1alpha-inducible protein, alters mitochondrial distribution and transport. J Cell Biol. Jun 15, 2009;185(6):1065-1081. [doi: 10.1083/jcb.200811033] [Medline: 19528298]

72. Monroe TB, Anderson EJ. A highly sensitive, reproducible assay for determining 4-hydroxynonenal protein adducts in biological material. Bio Protoc. Oct 5, 2019;9(19):e3383. [doi: 10.21769/BioProtoc.3383] [Medline: 33654879]

73. Mirzayans R, Murray D. Do TUNEL and other apoptosis assays detect cell death in preclinical studies? Int J Mol Sci. Nov 29, 2020;21(23):9090. [doi: 10.3390/ijms21239090] [Medline: 33260475]

74. Kraupp BG, Ruttkay-Nedecky B, Koudelka H, Bukowska K, Bursch W, Schulte-Hermann R. In situ detection of fragmented DNA (TUNEL assay) fails to discriminate among apoptosis, necrosis, and autolytic cell death: a cautionary note. Hepatology. May 1995;21(5):1465-1468. [doi: 10.1002/hep.1840210534] [Medline: 7737654]

75. Moore CL, Savenka AV, Basnakian AG. TUNEL assay: a powerful tool for kidney injury evaluation. Int J Mol Sci. Jan 2, 2021;22(1):412. [doi: 10.3390/ijms22010412] [Medline: 33401733]

76. Garrett-Bakelman FE, Darshi M, Green SJ, Gur RC, Lin L, Macias BR, et al. The NASA Twins Study: a multidimensional analysis of a year-long human spaceflight. Science. Apr 12, 2019;364(6436):eaau8650. [doi: 10.1126/science.aau8650] [Medline: 30975860]

77. Overbey EG, Das S, Cope H, Madrigal P, Andrusivova Z, Frapard S, et al. Challenges and

considerations for single-cell and spatially resolved transcriptomics sample collection during spaceflight. Cell Rep Methods. Nov 21, 2022;2(11):100325. [doi: 10.1016/j.crmeth.2022.100325] [Medline: 36452864]

78. Ong J, Lee AG, Moss HE. Head-down tilt bed rest studies as a terrestrial analog for spaceflight associated neuro-ocular syndrome. Front Neurol. Mar 26, 2021;12:648958. [doi: 10.3389/fneur.2021.648958] [Medline: 33841315]

79. Pandiarajan M, Hargens AR. Ground-based analogs for human spaceflight. Front Physiol. Jun 23, 2020;11:716. [doi: 10.3389/fphys.2020.00716] [Medline: 32655420]

80. Sarker P, Ong J, Zaman N, Kamran SA, Waisberg E, Paladugu P, et al. Extended reality quantification of pupil reactivity as a non-invasive assessment for the pathogenesis of spaceflight associated neuro-ocular syndrome: a technology validation study for astronaut health. Life Sci Space Res (Amst). Aug 2023;38:79-86. [doi: 10.1016/j.lssr.2023.06.001] [Medline: 37481311]

81. Waisberg E, Ong J, Zaman N, Paladugu P, Kamran SA, Tavakkoli A, et al. The spaceflight contrast sensitivity hypothesis and its role to investigate the pathophysiology of spaceflight-associated neuro-ocular syndrome. Front Ophthalmol (Lausanne). Sep 5, 2023;3:1229748. [doi: 10.3389/fopht.2023.1229748] [Medline: 38983005]

82. Scott RT, Sanders LM, Antonsen EL, Hastings JJA, Park S, Mackintosh G, et al. Biomonitoring and precision health in deep space supported by artificial intelligence. Nat Mach Intell. Mar 2023;5(3):196-207. [doi: 10.1038/s42256-023-00617-5]

83. Sanders LM, Scott RT, Yang JH, Qutub AA, Garcia Martin H, Berrios DC, et al. Biological research and self-driving labs in deep space supported by artificial intelligence. Nat Mach Intell. Mar 2023;5(3):208-219. [doi: 10.1038/s42256-023-00618-4]